Earth and Planetary Science Letters 303 (2011) 71–83

Contents lists available at ScienceDirect

Earth and Planetary Science Letters

journal homepage: www.elsevier.com/locate/epsl

Spatial controls on erosion in the Three Rivers Region, southeastern Tibet and southwestern China

Amanda C. Henck *, Katharine W. Huntington, John O. Stone, David R. Montgomery, Bernard Hallet

Department of Earth and Space Sciences and Quaternary Research Center, University of Washington, 070 Johnson Hall, Box 351310, Seattle, WA 98195-1310, United States

ARTICLE INFO

Article history:
Received 15 February 2010
Received in revised form 13 December 2010
Accepted 18 December 2010
Available online 20 January 2011

Editor: T.M. Harrison

Keywords:
Three Rivers Region
basin wide erosion rates
tectonic geomorphology
China
Eastern Tibet

ABSTRACT

Global data suggest that erosion rates variously scale with steepness or climate forcing (precipitation or glacial excavation), but the relative influence of these factors has proven difficult to assess without comparisons from a single location. A new suite of detrital ^{10}Be data from the Three Rivers Region, SE Tibet is used to examine the relative importance of rainfall and relief in predicting patterns of erosion rates across a region with a strong gradient in exhumation. The data reveal millennial erosion rates vary by two orders of magnitude, from 0.01 to 8 mm/yr across a regional gradient in exhumation rates inferred from previous thermochronology and cosmogenic nuclide data to the west and east of the study region. The new millennial erosion rates mirror the pattern of decreasing exhumation rates from west to east across the region, with the highest rates in the lower Salween River drainage and the lowest rates in the Yangtze River drainage. Erosion rates in the Mekong and Salween River drainages are correlated with mean local relief whereas in the Yangtze River drainage they are correlated most strongly with mean annual rainfall. The tectonic setting of this region, with a strong west to east gradient in exhumation rates which we infer to mirror a gradient in rock uplift, seems to exert a stronger control on erosion rate patterns than rainfall or relief.

1. Introduction

According to conventional geomorphological views, erosion rates generally increase with the steepness of hillslopes, as measured by mean local relief (Ahnert, 1970) up to a limiting or threshold slope (Montgomery and Brandon, 2002; Roering et al., 1999) at which point increased frequency of landslides increases erosion rates without further steepening hillslopes, or with the capacity of rivers to transport sediment and incise bedrock, as often estimated using stream power (Finlayson et al., 2002; Finnegan et al., 2005; Whipple and Tucker, 1999). Some workers have proposed that regional gradients in rainfall control spatial variations in erosion rates more than hillslope steepness or stream power (Anders et al., 2006; 2008; Montgomery et al., 2001; Reiners et al., 2003), whereas others have stressed that in tectonically active areas, the coupling of tectonic activity with erosion is strong enough to dominate the spatial pattern of erosion rates (Burbank et al., 2003; Finnegan et al., 2008; Zeitler et al., 2001).

Recent advances in cosmogenic nuclide dating have enabled direct measurement of erosion rates over millennial timescales (10^2 to 10^5 yrs depending on erosion rate) in a variety of geologic settings around the world (e.g., see compilation in von Blanckenburg, 2005). Taken broadly, no coherent relationship emerges between relief or rainfall and erosion rate in these studies except that erosion tends to be faster where tectonic uplift rates are higher (von Blanckenburg, 2005). Examining the relationship between erosion rate and relief or rainfall patterns in light of the relative long-term rate of rock uplift in each study region gives some insight which is helpful in reconciling the diverse results reported in previous studies. Many of the studies that suggest rainfall is a strong predictor of basin-averaged erosion rates are based in regions with relatively low rates of tectonically-driven rock uplift, such as Australia (Bierman and Caffee, 2002; Tomkins et al., 2007), the Cascades (Reiners et al., 2003), the Alps (Champagnac et al., 2009; Demoulin et al., 2009; Wittmann et al., 2007), the Eastern Cordillera of Columbia (Mora et al., 2008), and the Sierra Nevada (Dixon et al., 2009). In contrast, studies which suggest that relief or hillslope steepness is the major predictor for erosion rate patterns are primarily based in tectonically active areas such as the San Bernardino Mountains (Binnie et al., 2007), the Himalaya (Vance et al., 2003), northeastern Tibet (Harkins et al., 2007), and the Andes (Aalto et al., 2006; Barnes and Pelletier, 2006; Safran et al., 2005). Following Montgomery and Brandon (2002), other studies in tectonically active areas such as the Flinders Range (Quigley et al., 2007), the Apennines (Cyr and Granger, 2008), the Himalaya (Burbank et al., 2003; Finnegan et al., 2008), the Kun Lun Shan (Lal et al., 2004), Sichuan (Ouimet et al., 2009), and northwestern Tibet (Kong et al., 2007) note a limit to hillslope steepness and mean local relief and therefore independence between relief and erosion rates above a critical value. This independence is inferred to be a signature of strong tectonic control on erosion rates. In general these studies suggest the hypothesis that in areas with high rates of rock uplift, some measure of steepness (i.e., mean

* Corresponding author. Tel.: +1 206 651 5841.
E-mail addresses: achenck@uw.edu (A.C. Henck), kate1@uw.edu (K.W. Huntington), stone@geology.washington.edu (J.O. Stone), dave@ess.washington.edu (D.R. Montgomery), hallet@uw.edu (B. Hallet).

0012-821X/$ – see front matter © 2010 Elsevier B.V. All rights reserved.
doi:10.1016/j.epsl.2010.12.038

local relief or hillslope or river gradients) is the best predictor of erosion rate patterns up to a critical value while in areas with relatively low rates of uplift, rainfall is the best predictor of variance in erosion rates.

Taken at face value, the results of these studies may suggest the rate of tectonically-driven rock uplift is an important factor in determining the relative influence of climate-driven precipitation patterns and the form of the landscape itself (i.e., steepness, relief) on patterns of erosion. However, existing evidence in support of this hypothesis is difficult to evaluate because the erosion rate data discussed above were compiled from diverse landscapes all over the globe. In this study, we examine the relative importance of rainfall and relief in predicting millennial basin-wide erosion rates across a strong gradient in rock uplift rate in a single locality, the Three Rivers Region (TRR) in western China (Fig. 1a).

1.1. Tectonic setting and exhumation in the TRR

Located at the eastern limit of the India–Eurasia collision and southeastern margin of the Tibetan plateau, the TRR is defined by the elongate, roughly parallel drainages of the Salween (Nu Jiang), Mekong (Lancang Jiang), and Yangtze (Jinsha Jiang) Rivers. Previous studies of exhumation and millennial erosion rates suggest a gradient in exhumation and erosion across the TRR, which we interpret as a likely gradient in tectonically-driven rock uplift with respect to the geoid. To distinguish between short-term and long-term rates, we use 'erosion' for $\leq 10^5$-year rates of denudation and 'exhumation' for million-year rates. Below we review the TRR geology and evidence for a gradient in rock uplift across the region.

The great orogenic bend that defines the TRR at the northeast corner of the indenting Indian plate marks the abrupt transition between the east–west trending thrusts of the Himalaya and right-lateral strike–slip structures accommodating the northward motion of India relative to China (Burg et al., 1997). Crustal strain and thickening associated with ongoing India–Eurasia collision since the early Cenozoic has resulted in bending of structural fabrics, topography, and plate velocity vectors around the eastern Himalayan syntaxis (the Namche Barwa Area) (Hallet and Molnar, 2001; Royden et al., 1997; Sol et al., 2007; Tapponnier et al., 2001; Zhang et al., 2004). This rotation, which can be seen clearly in modern GPS data for the region (Zhang et al., 2004), has resulted in Indochina being extruded to the south along the Saqiang Fault, Chongshan shear zone, Gaoligong Shan shear zone, and the Ailao Shan shear zone complex (Akciz et al., 2008; Gilley et al., 2003; Harrison et al., 1992; Lacassin et al., 1996; Leloup and Kienast, 1993; Leloup et al., 1995, 2001; Scharer et al., 1990). Large parts of these shear zones are in the lower TRR.

At the largest scale, the TRR comprises the Lhasa Terrane in the Salween watershed, the Qiangtang Terrane in the Mekong and western Yangtze watershed, and the Songpan Ganzi Fold Belt in the eastern Yangtze watershed (Fig. 1b) (USGS, 2001). The Lhasa Terrane is primarily a shallow marine clastic sedimentary sequence of Ordovician and Carboniferous to Triassic age (Yin and Harrison, 2000). The Qiangtang Terrane (in the north) and Lanping–Simao Group (in the south; Fig. 1c) are divided from the Lhasa Terrane by the Bangong Suture (mélange and ophiolites). The Qiangtang Terrane and Lanping–Simao Group are made up of a thick layer of nonmarine Jurassic to early Cenozoic redbeds (Akciz et al., 2008) interstratified with low to high grade metamorphic rocks (Yin and Harrison, 2000). The Songpan–Ganzi Fold Belt is separated from the Qiangtang Terrane by the Jinsha Suture. The Fold Belt comprises a thick sequence of deep marine Triassic strata, often called the Songpan–Ganzi Flysch, that were intensely deformed during the late Triassic and early Jurassic by folding and thrusting (Yin and Harrison, 2000) and includes the Triassic Arc volcanics (Fig. 1c; Akciz et al., 2008).

While the TRR is dominated by sedimentary rocks in the upper watersheds, a mixture of sedimentary rocks and deeply exhumed metamorphic rocks are present in the lower watersheds. Much of the lower TRR is characterized by intensely sheared metamorphic rocks in the Ailao Shan shear zone complex (Akciz et al., 2008). The Ailao Shan shear zone complex is marked by four metamorphic cores, two of which are in the lower TRR (the Xuelong Shan and Diancang Shan massifs) (Leloup et al., 1995). These metamorphic cores are intensely sheared and contain deeply exhumed metamorphic rocks including paragneisses, augen gneisses, skarns, leucocratic melt layers, micaschists, hornblende schists, marbles, and migmatitic gneisses (Leloup et al., 1995). To the west of the Ailao Shan shear zone complex, the Gaoligong Shan shear zone contains amphibole grade gneisses (Akciz et al., 2008). Farther to the west, the Gaoligong Shan shear zone also contains deeply exhumed metamorphic rocks including migmatite-rich sections with abundant garnets, potassium feldspar, sillimanite, muscovite, biotite, quartz, and plagioclase (Akciz et al., 2008).

The active structures in the TRR include the Ganzi Fault system (a left-slip strike–slip system in the northern Yangtze watershed), a series of normal faults in the upper Yangtze and Salween watersheds, and some small normal and left-slip faults in the eastern lower-Yangtze (Fig. 1a; Taylor and Yin, 2009). The most active fault in the TRR is the north-striking Ganzi Fault system, which GPS data show to have significant modern left-slip motion (Taylor and Yin, 2009). Thus there is little active faulting identified in the region, with the exception of strike–slip faults in the upper and eastern Yangtze watersheds, which would be unlikely to dominate regional erosion patterns.

Spatial variations in the extent of a low-relief landscape in eastern Tibet provide one line of evidence for a regional gradient in exhumation rates. Eastern Tibet is characterized by a low-relief surface which has been inferred to be either a relict erosional surface uplifted during formation of the Tibetan Plateau (Clark and Royden, 2000; Clark et al., 2004, 2005a,b, 2006; Royden et al., 1997; Schoenbohm et al., 2004, 2006a,b) or deep basin-fill formed between the time when the region was uplifted and when the rivers had sufficiently eroded upstream and reconnected the ocean base-level to the Plateau surface (Liu-Zeng et al., 2008). The degree of incision into this low-relief surface provides a clue for the pattern of exhumation rates across the region. In the TRR, the upper reaches are not incised into the low-relief surface while the lower watersheds of the Mekong and Salween have fully eroded away this surface. Remnants of this low relief surface extend into the eastern part of the lower Yangtze watershed (Clark et al., 2005b, 2006), suggesting less exhumation, due to lower long-term exhumation rates or to a shorter duration of fluvial incision, in the Yangtze than the Mekong and Salween River drainages.

Previous thermochronometry data provide a second line of evidence for a gradient in exhumation rates across the region (Fig. 2). To the west, in the Namche Barwa region, exhumation rates as high as 10 mm/yr sustained for at least the last 1 to 10 Ma are indicated by numerous studies using a variety of thermochronometric techniques (Booth et al., 2004; Burg et al., 1997; Ding et al., 2001; Malloy, 2004; Seward and Burg, 2008). To the east of the TRR, exhumation rates inferred from biotite $^{40}Ar/^{39}Ar$, apatite and zircon U–Th/He, and apatite fission track thermochronometry from the incised portions of the landscape are reported between 0.25 and 0.65 mm/yr since 9–13 Ma (Clark et al., 2005b; Godard et al., 2009; Kirby et al., 2002; Ouimet et al., 2010). The ten-fold decrease in exhumation rates averaged over million-year timescales from west to east suggests a strong gradient in regional exhumation across the TRR. For such a high gradient in exhumation rates to have been sustained over the $\geq$10 Ma over which the rate estimates are averaged, there most likely exists a corresponding gradient in rock uplift across the TRR.

Erosion rates inferred from ^{10}Be analyses of river sands parallel this gradient in long-term exhumation rates (Fig. 2). Finnegan et al. (2008, data repository) report 1–4 mm/yr erosion in the Namche Barwa region while Ouimet et al. (2009) report erosion rates to the east of the TRR between 0.14 and 0.58 mm/yr in the incised parts of the landscape. These erosion rates are of the same order of magnitude as exhumation rates for the same regions, suggesting that millennial erosion rates in eastern Tibet broadly reflect local longer-term exhumation rates.

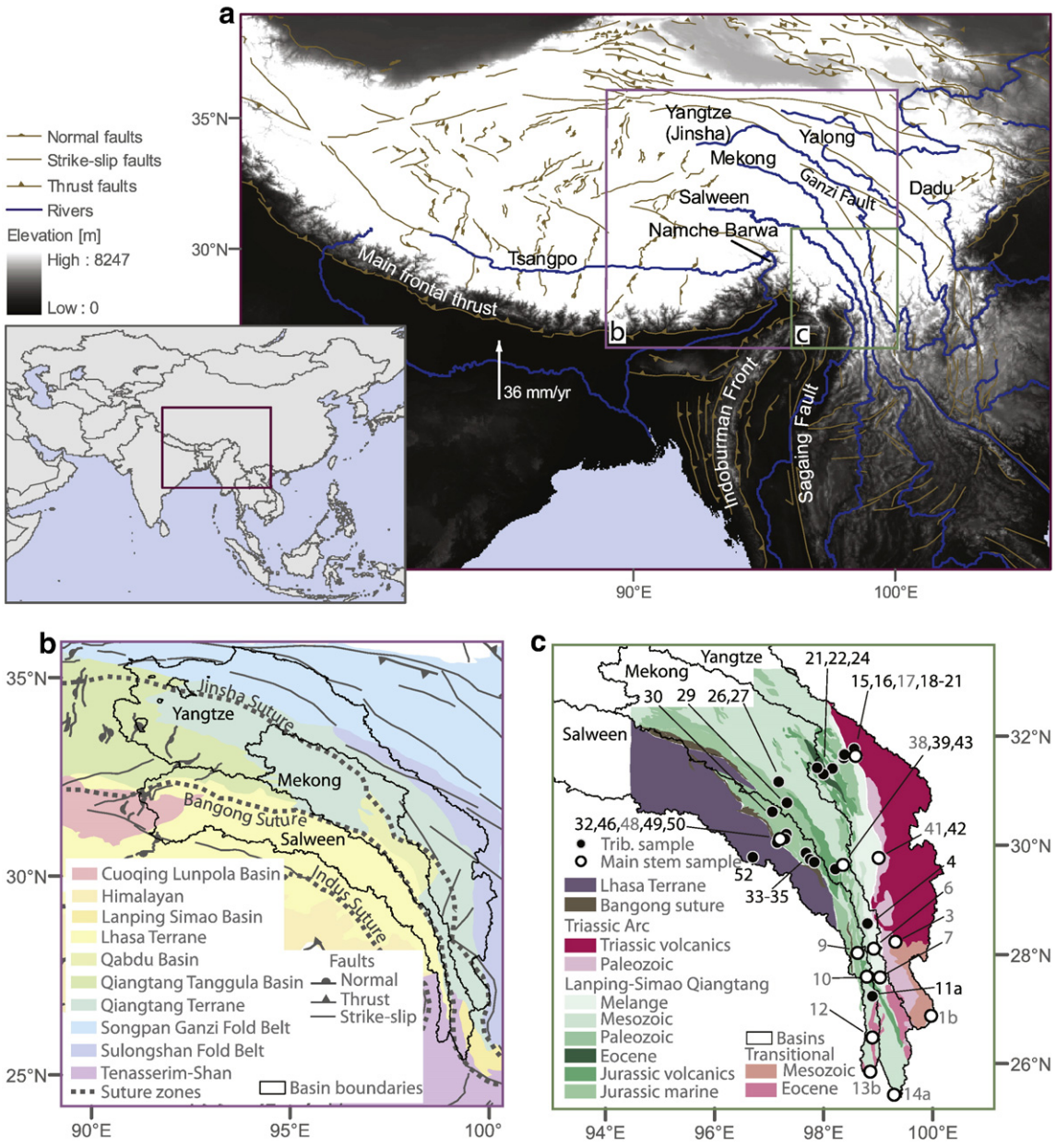

Fig. 1. Geologic and geomorphic setting of the TRR. (a) Context map of the study region showing major structures, topography, and major rivers. Fault data are from Taylor and Yin (2009). (b) Tectonic terranes (USGS, 2001) and faults in the vicinity of the TRR (Taylor and Yin, 2009). (c) Bedrock geology (modified from Akciz et al., 2008) and location of samples for the TRR. Main stem samples are noted by white circles with black outlines and grey text. Tributary samples are black circles with white outlines and black text. Sample numbers correspond to those given in tables and data repository.

2. Methods

2.1. Erosion rates from ^{10}Be

In order to quantify the spatial distribution of millennial erosion rates in the TRR, we calculated basin-wide erosion rates from measured cosmogenic ^{10}Be in modern stream sediments. Beryllium-10 is produced *in situ* when cosmic rays interact with the uppermost layer of Earth's surface, and is carried by detrital sediment after detachment and erosion. The concentration of ^{10}Be can be used to quantify basin-wide average erosion rates, as originally discussed by Brown et al. (1995), Bierman and Steig (1996), and Granger et al. (1996).

We analyzed *in-situ*-produced ^{10}Be in 45 samples of detrital quartz from sand collected in catchments of varying size (~2 km^2 to >300,000 km^2) throughout the TRR (Fig. 1c, Table 1). Instead of working with samples only from small tributary basins as is commonly done (see reviews by Bierman, 2004; von Blanckenburg, 2005), we collected samples from a wide range of main stem and tributary locations in each of the TRR basins. Twenty-seven samples were taken from main stem reaches of the Salween, Mekong and Yangtze, or from the lower reaches of major tributaries close to their junctions with these rivers. The remaining nineteen samples are from headwater tributaries. All samples were collected from active parts of the flood plain, or from sandbars immediately adjacent to rivers.

Samples were sieved and prepared using standard laboratory methods (Bierman, 2004; Kohl and Nishiizumi, 1992; Stone, 2004). To obtain the most representative sampling of the large catchments investigated, we extracted quartz from the 180–425 μm size fraction of most samples. The lower limit of 180 μm was selected because insufficient amounts of the finer grain size fractions survive the HF

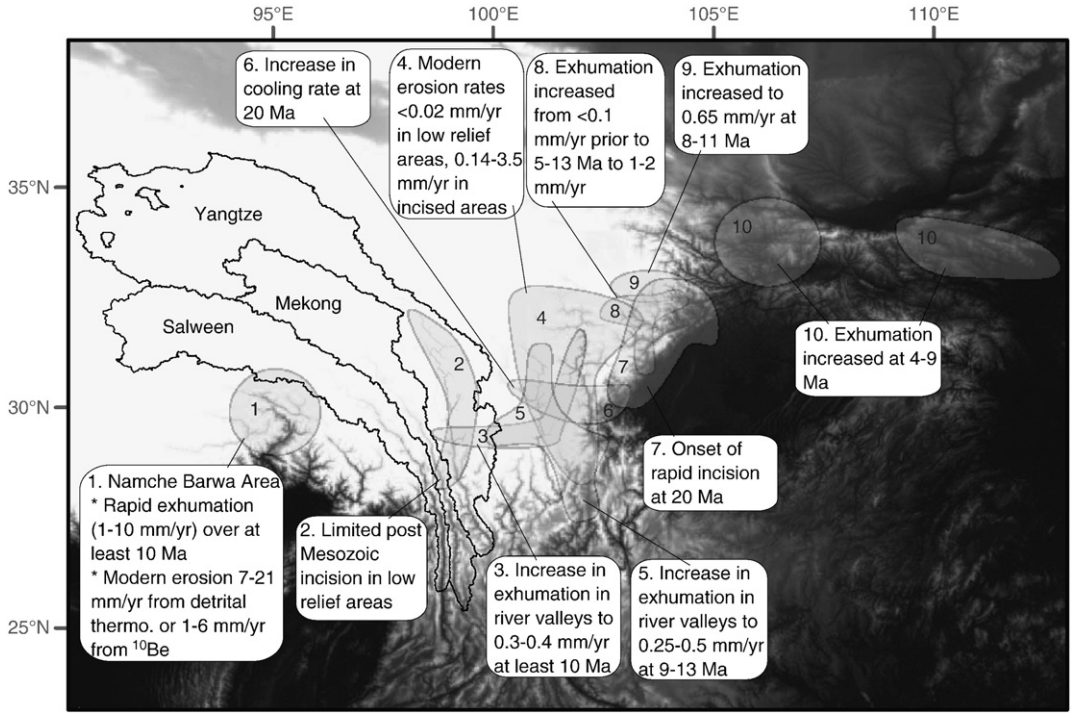

Fig. 2. Summary of previous work on erosion rates (areas 1 and 4) and exhumation rates (all other labels). Data for the Namche Barwa area (area 1) are from Burg et al. (1997), Ding et al. (2001), Booth et al. (2004), Malloy (2004), Seward and Burg (2008), Finnegan et al. (2008), and Stewart et al. (2008). Data for area 2 are from Reid et al. (2005), for area 3 from Ouimet et al. (2010), for area 4 from Ouimet et al. (2009), for area 5 from Clark et al. (2005b), for area 6 from Xu and Kamp (2000), for area 7 from Arne et al. (1997), for area 8 from Kirby et al. (2002), for area 9 from Godard et al. (2009), and for area 10 from Enkelmann et al. (2006). Across the TRR there is a clear decrease from west to east in exhumation rates and modern erosion rates which we infer as a probable decrease in uplift.

etching procedure used to concentrate and purify quartz. The upper limit of 425 μm was selected because many samples had only fine sand. Two headwater catchment samples contained insufficient 180–425 μm quartz for analysis, and thus we analyzed the 425–850 μm fraction. In three additional samples, one from the main stems of each of the Three Rivers, we measured *in-situ*-produced ^{10}Be in both the 180–425 μm and 180–850 μm fractions to evaluate potential effects of grain size on erosion rate estimates.

Beryllium isotopic measurements were made at PRIME laboratory, Purdue University, and erosion rates averaged over the contributing area upstream of each sample were calculated from the data using the CRONUS online calculator (Balco et al., 2008). Isotopic values reported in Table 2 are referenced to revised values of the KNSTD Be isotope standards (Nishiizumi et al., 2007), and erosion rates are calculated using the corresponding value of ^{10}Be half-life. The upstream basin information for each sample was calculated for basins defined by the WWF Hydrosheds data (USGS, 2008). The average ^{10}Be production rate for each basin was calculated using the standard procedure to account for latitude, longitude, and effective elevation (the elevation which will result in the correct basin-averaged production rate) for each basin (Balco, 2006).

First we calculated erosion rates for the entire upstream area of all samples using the CRONUS Online Calculator. Erosion rates for intermediate reaches between two samples on the same channel were then determined from the differences in erosion rate and contributing area of the successive samples (following Vance et al., 2003). Errors reported for the intermediate reaches are the sum of fully propagated internal (and independent) errors and the average external (and dependent) errors of contributing samples.

2.2. Potential indicators of erosion

Previous workers have suggested that the efficacy of surface processes responsible for erosion is enhanced as the modern rainfall rate or hillslope or river steepness (i.e., as measured by hillslope angles, river steepness corrected for a reference concavity, stream power, or mean local relief) increases as discussed in Section 1. As described in the following sections, we examine spatial patterns of both rainfall and steepness across the TRR and compare them to the observed pattern of millennial basin-averaged erosion rates.

2.2.1. Steepness — predicting erosion rate patterns using mean local relief

We use mean local relief as a measure of landscape steepness. Unlike channel slope, hillslope angle, or stream power, mean local relief does not require direct measurements of slope and is therefore less dependent on quality and scale of DEMs, but still has been shown to be well correlated with erosion rates worldwide (Montgomery and Brandon, 2002).

Ahnert (1970) proposed a simple linear function between erosion rates and local relief in mountainous areas:

$$E = 0.2R, \tag{1}$$

where E is erosion in mm/yr and R is local relief in km, averaged over the area for which E was measured. Montgomery and Brandon (2002) observed that in tectonically active areas, the erosion rate increases more rapidly for small increases in relief. They proposed that in such areas (i.e., in active orogenic settings characterized by rapid rock uplift) where hillslopes are steep, erosion rates increase primarily through increased frequency of landslides (Montgomery and Brandon, 2002). Their compilation of relief and erosion-rate data from tectonically active and other regions is well described by a power law:

$$E = 1.4 \times 10^{-6} R^{1.8}, \tag{2}$$

where R is in meters (Montgomery and Brandon, 2002).

Table 1
Details on location and sequence of samples used in analysis. The samples are named by year sample was collected (05 or 06), project (3R), watershed (SAL for Salween, MEK for Mekong, YANG for Yangtze), and a sample number (1 to 52). The same number is what corresponds to the sample numbers in Fig. 2.

Sample name	Details on collection location				Upstream area (km^2)
	Latitude	Longitude	River description	Samples upstream	
06-3R-52-SAL	29.78	96.71	Trib to Salween trib.	None	363
06-3R-50-SAL	30.04	97.15	Trib to Salween trib.	None	869
06-3R-49-SAL	30.11	97.19	Trib to Salween	06-3R-52-SAL, 06-3R-50-SAL	3108
06-3R-48-SAL	30.10	97.21	Salween	06-3R-49-SAL	283749
06-3R-46-SAL	30.10	97.30	Trib to Salween trib.	None	57
06-3R-30-SAL	30.60	97.07	Trib to Salween trib.	None	2136
06-3R-32-SAL	30.20	97.32	Trib to Salween trib.	06-3R-30-SAL	3280
06-3R-33-SAL	29.85	97.69	Trib to Salween trib.	None	251
06-3R-34-SAL	29.74	97.76	Trib to Salween trib.	06-3R-32-SAL, 06-3R-33-SAL	5787
06-3R-35-SAL	29.68	97.83	Trib to Salween trib.	None	131
05-3R-9-SAL	28.02	98.63	Salween	06-3R-34-SAL, 06-3R-35, SAL, 06-3R-46-SAL, 06-3R-48-SAL	303138
05-3R-10-SAL	27.58	98.79	Salween	05-3R-9-SAL	305003
05-3R-11a-SAL	27.23	98.89	Trib to Salween	None	2
05-3R-12-SAL	26.48	98.90	Salween	05-3R-10-SAL, 06-3R-11a-SAL	307894
05-3R-13b-SAL	25.85	98.86	Salween	06-3R-12-SAL	310028
06-3R-26-MEK	31.15	97.16	West branch of Mekong at Chamdo	None	16875
06-3R-27-MEK	31.15	97.18	East branch of Mekong at Chamdo	None	36710
06-3R-29-MEK	30.77	97.34	Trib to Mekong	None	6733
06-3R-38-MEK	29.62	98.35	Mekong	06-3R-26-MEK, 06-3R-27-MEK, 06-3R-29-MEK	73147
06-3R-39-MEK	29.66	98.37	Trib to Mekong	None	167
06-3R-43-MEK	29.55	98.21	Trib to Mekong	None	328
05-3R-4-MEK	28.56	98.81	Trib to Mekong	None	465
05-3R-6-MEK	28.10	98.92	Mekong	06-3R-38-MEK, 06-3R-39-MEK, 06-3R-43-MEK, 06-3R-4-MEK	77316
05-3R-7-MEK	27.57	99.04	Mekong	06-3R-6-MEK	80648
05-3R-14a-MEK	25.43	99.29	Mekong	06-3R-7-MEK	91031
06-3R-15-YANG	31.76	98.56	Trib to Yangtze	None	1376
06-3R-16-YANG	31.64	98.59	Trib to Yangtze	06-3R-15-YANG	1642
06-3R-17-YANG	31.63	98.59	Yangtze	06-3R-16-YANG	245160
06-3R-21-YANG	31.40	98.16	Trib to Yangtze trib.	None	1450
06-3R-20-YANG	31.59	98.37	Trib to Yangtze trib.	06-3R-21-YANG	1911
06-3R-19b-YANG	31.65	98.37	Trib to Yangtze trib.	None	1552
06-3R-19a-YANG	31.65	98.37	Trib to Yangtze trib.	06-3R-19a-YANG	1596
06-3R-18-YANG	31.62	98.60	Trib to Yangtze trib.	None	157
06-3R-22-YANG	31.30	98.00	Trib to Yangtze trib.	None	368
06-3R-24-YANG	31.40	97.88	Trib to Yangtze trib.	None	131
06-3R-41-YANG	29.76	99.00	Yangtze	06-3R-17-YANG, 06-3R-20-YANG, 06-3R-19a-YANG, 06-3R-18-YANG, 06-3R-22-YANG, 06-3R-24-YANG	277472
06-3R-42-YANG	29.76	99.01	Trib to Yangtze	None	617
05-3R-3-YANG	28.22	99.32	Yangtze	06-3R-41-YANG, 06-3R-42-YANG	300774
05-3R-1b-YANG	26.87	99.97	Yangtze	05-3R-3-YANG	310726

For our analysis, we calculated local relief for a 5 km radius window over 30″ SRTM-derived DEMs (USGS, 2008). The resulting local relief values were then used to calculate mean local relief for each of the basins for which we measured erosion rates.

2.2.2. Climate — predicting erosion rates from mean annual rainfall

We use modern mean annual rainfall as a measure of climatic variation across our study area. This parameter enables direct comparison of results with previous studies and allows us to use Tropical Rainfall Measuring Mission (TRMM) satellite data to calculate rainfall. We calculated mean annual rainfall patterns throughout the TRR using average annual precipitation for 1 km × 1 km pixels over 2000–2006 using the TRMM satellite data and the methods described by Anders et al. (2006). TRMM data are acquired on a schedule such that data are collected over all periods of a day but not all the time, capturing daily variability in rainfall but not the total amount of rainfall. As a result, the mean annual values we report likely underestimate actual rainfall but portray the spatial distribution of rainfall reasonably; errors are likely to range from 15 to 50% (Anders et al., 2006).

3. Results

Our results show parallel increases in basin-wide ^{10}Be erosion rates, mean local relief, and mean annual rainfall from north to south in the TRR. In contrast, in the lower basins where relief and rainfall are relatively uniform, erosion rates decrease two-orders of magnitude from west to east in concert with the inferred gradient in rock uplift.

3.1. Erosion rates from Be-10

Based on previous research in eastern Tibet (Fig. 2), we expect that erosion rates in the TRR will follow the broad patterns observed in erosion and exhumation rates in surrounding areas. Therefore, we expect that erosion rates will be lowest in unincised, low-relief parts of the Tibetan Plateau, such as the farthest upstream reaches of the TRR. Erosion rates are expected to increase as the rivers enter the incised gorges of the lower reaches. In addition to this general pattern of higher erosion rates in the more incised parts of the study area, we expect that erosion rates will decrease from west to east in parallel with decreases in exhumation and erosion rates measured in surrounding areas. Our data confirm both of these general trends — one of increasing erosion rates from north to south and the other of increasing erosion rates from east to west across the incised parts of the landscape (Table 2; Fig. 3).

Basin-averaged erosion rates in the Salween River drainage generally increase southward from 0.024 ± 0.005 mm/yr to a peak rate of 8 ± 3 mm/yr (Fig. 3b). The highest erosion rate estimate in this drainage is for the narrowest portion of the TRR between ~25 and 27°N (i.e., between 05-3R-13b-SAL and 05-3R-12-SAL). Similarly, although the peak erosion rates are lower, the Mekong River erosion rates increase southward from 0.017 ± 0.002 to a peak rate of 0.5 ±

Table 2
Concentrations of ^{10}Be and derived erosion rates for entire upstream basins (a) and intermediate reaches between samples (b).

a)

Sample name	N (atoms/g)	Error in N atoms/g	Erosion rate (mm/yr)	Error (mm/yr) 95% confidence
06-3R-52-SAL	277111	14909	0.22	0.03
06-3R-50-SAL	105850	5784	0.55	0.08
06-3R-49-SAL	231103	10285	0.24	0.03
06-3R-48-SAL	784949	20449	0.070	0.008
06-3R-46-SAL	367464	15764	0.12	0.016
06-3R-30-SAL	2078252	62058	0.026	0.003
06-3R-32-SAL	2120444	58616	0.025	0.003
06-3R-33-SAL	1553608	50391	0.034	0.004
06-3R-34-SAL	1092820	26768	0.048	0.005
06-3R-35-SAL	1237683	50806	0.041	0.006
05-3R-9-SAL	518500	12296	0.11	0.011
05-3R-10-SAL	427659	11859	0.13	0.015
05-3R-11a-SAL	161438	7129	0.08	0.010
05-3R-12-SAL	402267	15524	0.13	0.017
05-3R-13b-SAL	294362	12158	0.18	0.02
06-3R-26-MEK	317841	9684	0.18	0.02
06-3R-27-MEK	432965	12691	0.12	0.014
06-3R-29-MEK	678376	26294	0.08	0.010
06-3R-38-MEK	352113	10049	0.14	0.017
06-3R-39-MEK	344713	14531	0.11	0.015
06-3R-43-MEK	2768030	67592	0.017	0.002
05-3R-4-MEK	70117	5195	0.57	0.10
05-3R-6-MEK	308766	17071	0.16	0.02
05-3R-7-MEK	295439	12621	0.17	0.02
05-3R-14a-MEK	261412	14464	0.17	0.03
06-3R-15-YANG	360619	11421	0.13	0.016
06-3R-16-YANG	384297	13299	0.12	0.015
06-3R-17-YANG	4063015	59101	0.014	0.001
06-3R-21-YANG	949300	36916	0.048	0.006
06-3R-20-YANG	948113	30610	0.048	0.006
06-3R-19b-YANG	924199	20444	0.049	0.005
06-3R-19a-YANG	651735	29344	0.07	0.010
06-3R-18-YANG	360839	26401	0.12	0.021
06-3R-22-YANG	782810	33147	0.058	0.008
06-3R-24-YANG	881427	39199	0.060	0.008
06-3R-41-YANG	3262761	97513	0.017	0.002
06-3R-42-YANG	984334	38432	0.043	0.006
05-3R-3-YANG	2814015	45255	0.019	0.002
05-3R-1b-YANG	2661264	52493	0.020	0.002

b)

Sample name	Area (sq. km)	Erosion rate (mm/yr)	Error (mm/yr) 95% confidence
06-3R-49-SAL	1876	0.10	0.03
06-3R-48-SAL	280641	0.068	0.01
06-3R-32-SAL	1144	0.024	0.00
06-3R-34-SAL	2255	0.082	0.01
05-3R-9-SAL	13563	0.9	0.14
05-3R-10-SAL	1716	4	1.12
05-3R-12-SAL	3038	0.8	0.80
05-3R-13b-SAL	1985	8	2.13
06-3R-38-MEK	12830	0.22	0.03
05-3R-6-MEK	5067	0.4	0.40
05-3R-7-MEK	1474	0.5	0.66
05-3R-14a-MEK	10383	0.2	0.12
06-3R-16-YANG	266	0.07	0.04
06-3R-17-YANG	244894	0.0126	0.001
06-3R-20-YANG	461	0.047	0.01
06-3R-19a-YANG	45	0.8	0.19
06-3R-41-YANG	26774	0.042	0.01
05-3R-3-YANG	20546	0.04	0.01
05-3R-1b-YANG	11056	0.04	0.02

0.7 mm/yr (Fig. 3c). As with the Salween River, the peak erosion rates in the Mekong River drainage are for the narrowest portion of the TRR between ~25 and 29°N (i.e., between 05-3R-14a-SAL and 06-3R-38-MEK). The Yangtze River drainage also follows this pattern of increasing erosion rates to the south of the basin with erosion rates increasing from 0.013 ± 0.001 mm/yr to a peak of 0.04 ± 0.01 mm/yr in the southern reaches of the main stem (i.e., between 05-3R-1b-YANG and 06-3R-17-YANG; Fig. 3d). Unlike the Mekong and Salween river drainages, the highest erosion rates in the Yangtze River drainage are in small tributaries which are deeply incised into the low-relief plateau surface rather than along the main stem of the river (i.e., 06-3R-19a-YANG).

The peak erosion rates vary greatly across the study area, although all three rivers follow a general pattern of increasing erosion rate

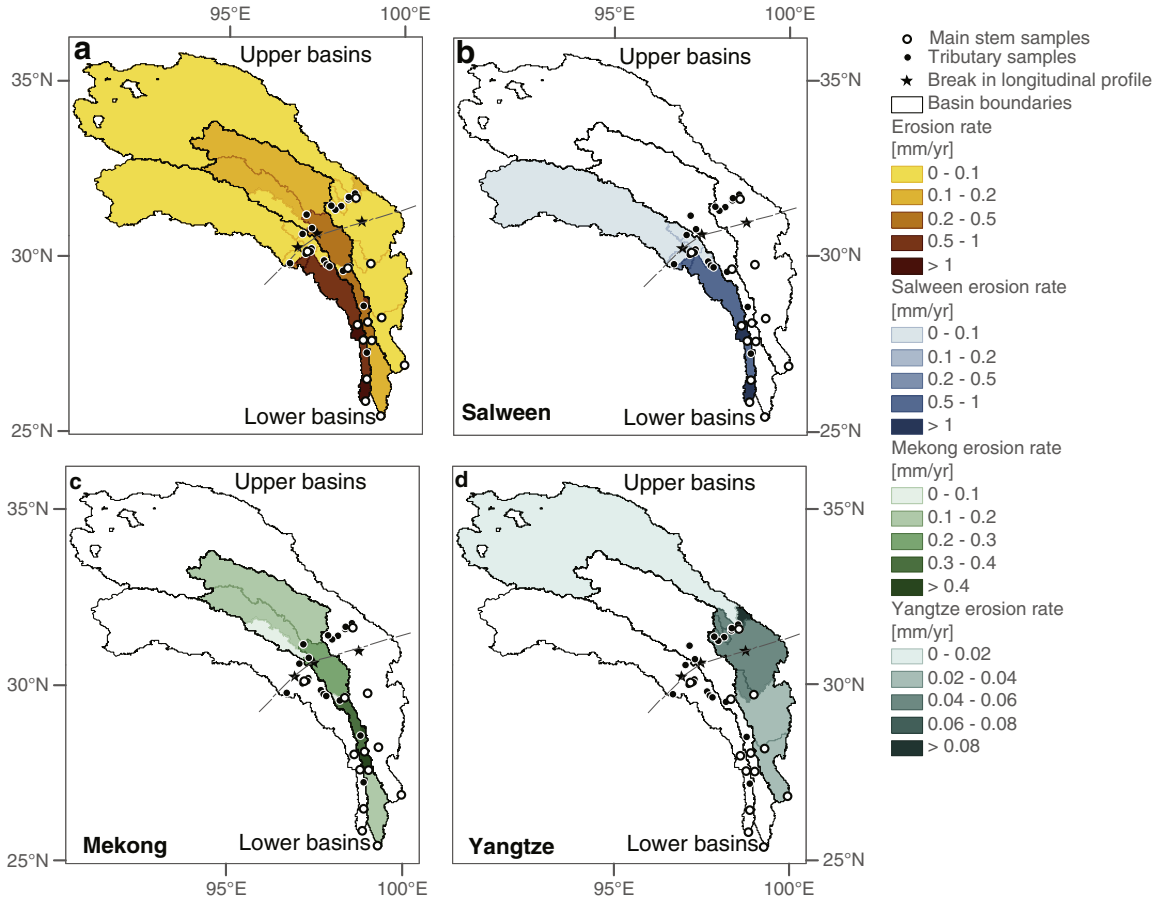

Fig. 3. Erosion rates measured for the TRR are shown for the region as a whole and for each individual basin. Break in longitudinal profile where the slope of each river increases, corresponding with the river leaving the Tibetan Plateau, is marked with a line which divides each basin into an upper and lower basin. For each watershed there is a trend in increasing erosion rate as the rivers move from the relatively flat Tibetan Plateau into the deeply dissected gorges of the TRR. There is also an across-basin trend in the lower basins where erosion rate decreases sharply from the Salween to Yangtze Rivers.

southward after leaving the low-relief plateau surface and entering the incised gorges of their lower reaches. These peak rates are 8 ± 3, 0.5 ± 0.7 and 0.04 ± 0.01 mm/yr respectively for the main stems of the Salween, Mekong and Yangtze rivers. This two-order of magnitude decrease in erosion rates across the lower basins of the TRR is parallel to, and the same order of magnitude as, the decrease in exhumation and erosion rates measured to the east and west of the TRR.

In order to confirm that limiting the range of grain sizes analyzed does not significantly impact our results, we measured ^{10}Be in two different grain size fractions (180–850 μm and 180–425 μm) for three samples. In all cases the difference in rate estimated for the two size fractions is less than the spread of rate estimates based on duplicate 180–425 μm preparations of sample 06-3R-27-MEK ($3.8 \pm 0.1 \times 10^5$ *vs.* $4.3 \pm 0.1 \times 10^5$ atoms ^{10}Be/g), and corresponds to negligible (± 0.01 mm/yr for 05-3R-11b-SAL and 06-3R-26-MEK and ± 0.001 mm/yr for 05-3R-17-YANG) differences in apparent erosion rate. For consistency with the rest of the data set we refer to the results from the 180–425 μm fractions of these samples in the following discussion and calculations. In the case of the duplicate analyses the same grain size of sample 06-3R-27-MEK, which yielded erosion rates within analytical error of each other, we favor the lower ^{10}Be concentration because it implies an erosion rate that is compatible with samples upstream.

As mentioned in Section 2.1, for each watershed we sampled both tributaries and several samples successively downstream on the main stem channels. When sampling successive samples in this way, it is possible that a sample will not be representative of the upstream area and thus will yield erosion rates for intermediate reaches which do not make sense. To confirm that successive samples on the main stem of rivers are representative of the upstream area, we analyzed the trends in cumulative sediment yield measured along each river. For erosion rates to be valid, the cumulative sediment yield must increase with each successive downstream sample. The cumulative sediment yield (erosion rate times upstream area) increases within measurement errors downstream along the main stem of each of the three rivers (Fig. 4), suggesting that the samples are indeed representative of the average erosion rate for the region (see supplemental material for a more detailed discussion of the validity of our erosion rate measurements).

3.2. Patterns of local relief and mean annual precipitation

In parallel with the increase in erosion rates with increasing distance downstream in the watersheds, the highest values of local relief and mean annual rainfall generally are restricted to the narrowest parts of the TRR drainage (Fig. 5). To highlight overall regional trends in local relief and precipitation across the TRR, we present values of these variables over the entire region. Basin averaged values are used for correlation analysis with erosion rates (Section 2.2).

The overall range of local relief in the TRR is 50 m to 3000 m, with the areas of highest local relief being found along the main stems of the Salween, Mekong, and Yangtze Rivers (Fig. 5a), especially along the narrowest sections of the TRR, between 24 and 30°N in the Salween basin, and north of 26°N in the Mekong basin. These areas correspond to regions where the low-relief surface has been

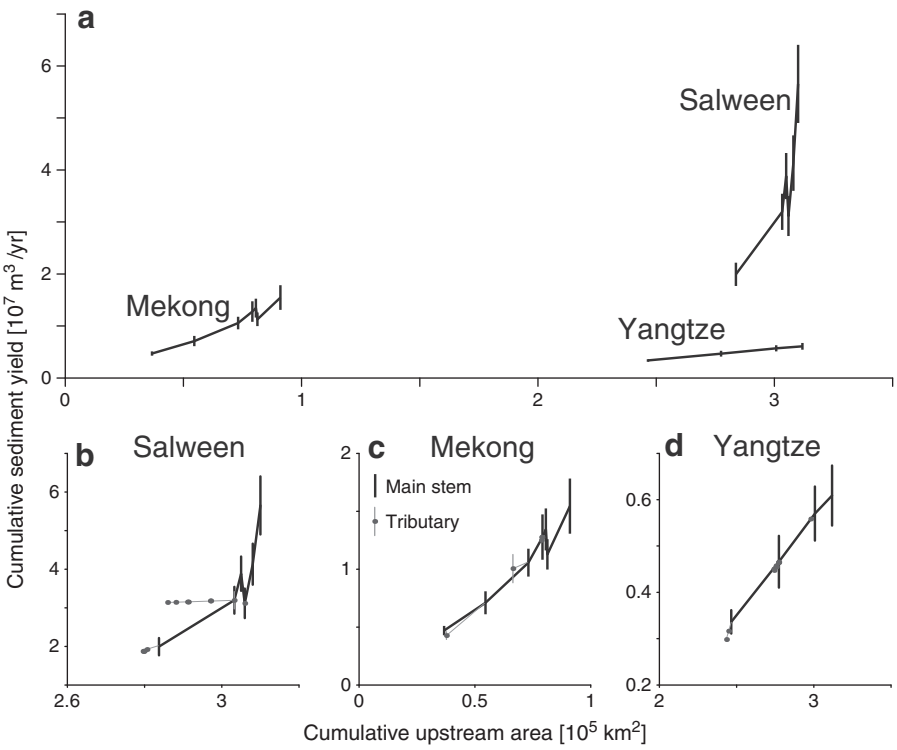

Fig. 4. (a) Downstream increase in cumulative sediment yield along the mainstems of the Salween, Mekong and Yangtze rivers. Plot shows cumulative sediment yield (the product of erosion rate and drainage area) *vs* the basin area upstream of each sample point. In this representation the erosion rate of the reach (and tributaries) between any pair of mainstem samples is given by the slope of the line between them, and the average erosion rate of the basin above the highest sample is the slope of the line joining that sample point to the origin. The plot clearly shows the contrast in erosion rates between the three rivers, and the increase in the erosion rates of the Mekong and Salween as they leave the Tibetan Plateau and flow into their incised gorges. (b–d) Detail of the curve for each river. Note the different scales for these three plots. Note also that points representing tributary basins on the detailed diagrams (small dots) are plotted such that the x-offset from the mainstem curve gives the tributary basin area, and the slope gives the tributary basin erosion rate. This allows comparison between tributary and mainstem erosion rates. However, when plotted this way the y-values for the tributary points do not correspond to actual cumulative sediment yields.

completed eroded (Clark et al., 2005b; 2006). Local relief in the Yangtze River basin remains high from the southern limit of the Yangtze drainage in the study area (27°N to 34°N), but is slightly lower to the far eastern edge of the basin, corresponding to an area where the low-relief surface has not been incised (Clark et al., 2005b, 2006).

The mean annual rainfall in the TRR varies by a factor of five, from less than 250 mm/yr to nearly 1200 mm/yr (Fig. 5b). Generally, annual precipitation decreases to the north and east of the peak rainfall areas. The southern reaches of the Salween and Mekong Rivers (south of 27°N and 26°N, respectively) receive the highest annual precipitation of any of the main stem channels of the TRR. The northernmost regions of the Yangtze (north of ~33°N) are the driest. Along the main stem of the Salween, the rainfall increases downstream three-fold from 380 mm/yr to over 1190 mm/yr across a distance of 500 km. Mean annual rainfall along the Mekong River is also variable and increases from 430 mm/yr in the northern reaches to 1000 mm/yr in the southern reaches. In the far south of the TRR, there is a modest decrease in rainfall from west to east (1160 to 980 mm/yr).

4. Discussion

Below we consider whether variations in lithology or river incision could explain our observed erosion rates, the relative influence of climate and topography on erosion rates, and potential geomorphic mechanisms which could produce and maintain the erosion rates we observe over short timescales. Of most interest to our analysis of the relative influence of climate and topography on erosion are the details of how erosion rates vary as a function of proxies for climate (mean annual rainfall) and steepness (mean local relief) within the context of the regional gradient in rock uplift. We find that rainfall best explains variance in erosion rates in the Yangtze watershed while variance in erosion rates is best explained by mean local relief in the Mekong and Salween watersheds, supporting the hypothesis that rock uplift rate is important in dictating whether climate or steepness is the most significant parameter for predicting variance in erosion rates.

4.1. Potential influence of lithology and differential river incision on measured erosion rates

Lithology is a potentially strong control on fluvial incision rates (Stock and Montgomery, 1999) and may be as strong as variation in rock uplift rates (Duvall et al., 2004). Thus, it is possible that both the downstream and east to west increase in erosion rates are due to changing lithology from more resistant to more erosive rocks. However, Figs. 1b and 1c and the discussion of lithology in Section 1.1 suggest that lithology varies widely throughout the watershed. The only systematic trend in lithology across the region is that the more deeply exhumed, resistant metamorphic rocks are in the southern parts of the TRR while the generally less resistant sedimentary rocks are in the northern reaches. Thus if lithology were the dominant control on erosion, we would expect lower erosion rates to the south than to the north — the opposite of the trend in erosion rates we observe. In addition, there is no systematic east to west gradient in the distribution of weak and strong lithologies. This suggests that the large east–west gradient in erosion rates in the southern part of the TRR is independent of lithology.

Similarly, differential incision of the low-relief surface (Clark et al., 2006; Liu-Zeng et al., 2008) may explain spatial patterns of erosion in the TRR. Areas with less incision should have lower basin-wide erosion rates than those with more incision, depending on the amount

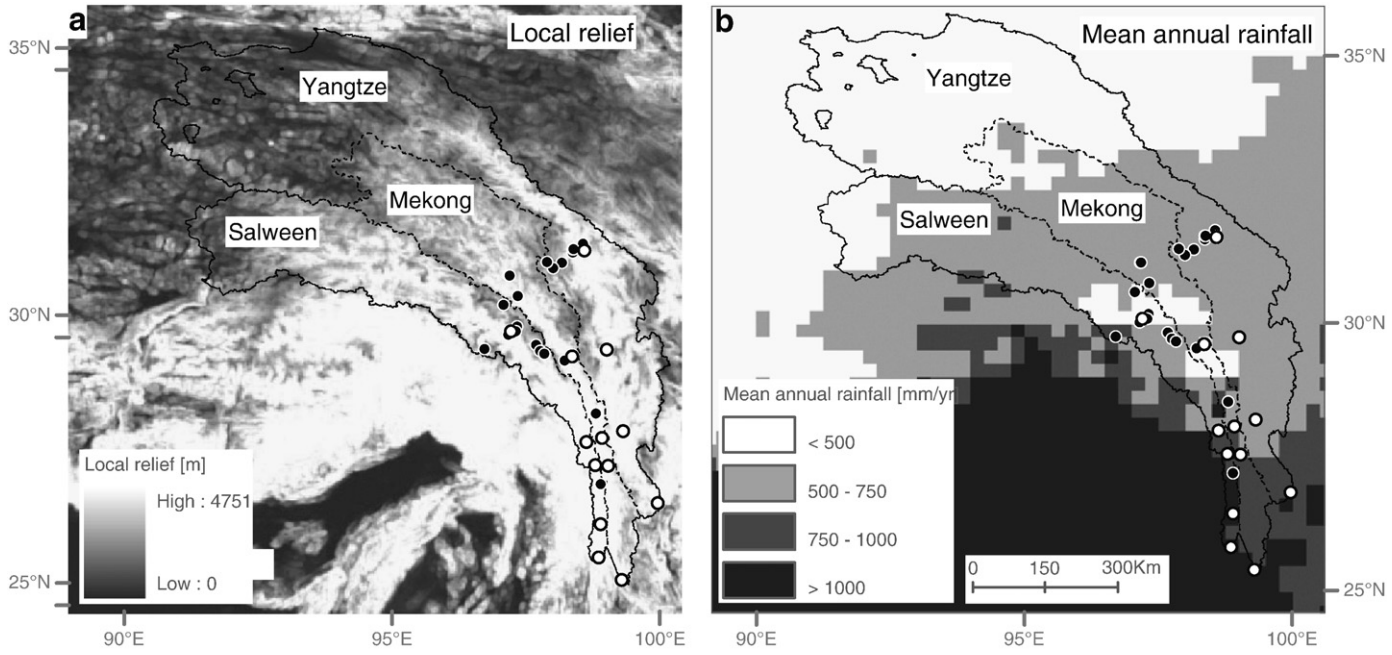

Fig. 5. (a) Steepness (mean local relief) and (b) climatic (mean annual rainfall) parameters for the region.

of sediment contributed by the slowly eroding, low relief surface. The headwater regions of the TRR have the largest areas of low-relief surface, suggesting that they should have the lowest erosion rates. To the south, the rivers are deeply incised in gorges, which should have higher erosion rates. This is the pattern we observe, suggesting the north to south increase in erosion rates in the TRR reflect, at least in part, differential river incision. Less of the low-relief surface is preserved in the Salween drainage than in the Mekong and Yangtze drainages (Clark et al., 2006), pointing to differential incision as a possible explanation for the east to west decrease in basin-wide erosion rates as well. However, the difference in degree of river incision is minor across the lower basins, as indicated by the relatively uniform local relief (Fig. 5). Thus, although it is possible that much of the spatial variation in erosion rates observed in the TRR is a reflection of differential incision into the low-relief surface, we suggest the measured erosion rates in the lower TRR are mostly reflective of the fully incised landscape.

4.2. Relief and rainfall as indicators of erosion rates

Taking the TRR as a whole, climatic and steepness parameters are comparable predictors of patterns of erosion rates ($r^2 = 0.41$, 0.48, $p < 0.01$ for rainfall and relief, respectively; Fig. 6 a–b). Both rainfall and relief explain between 40 and 50% of the observed variance in erosion rates. Combining the predictive powers of mean annual rainfall and mean local relief increases the predictive power of these parameters to nearly 60% of the variance ($r^2 = 0.56$, $p < 0.01$; see data repository Table 5 for all of the r^2 and p values for single and multiple regressions). Erosion rates are independent of basin area ($r^2 = 0.01$, $p = 0.40$; Fig. 6c).

We analyzed independently the predictive power of rainfall and relief on erosion rates for each river drainage. All three rivers exhibit increasing erosion rates with increasing distance downstream. However, there are subtle differences in which parameters best explain the spatial variance in erosion rates for each drainage. The variance in erosion rates in the Salween and Mekong River drainages are best explained by mean local relief ($r^2 = 0.75$, 0.46, $p < 0.01$, respectively; Fig. 6d–e), as is the case for many watersheds in regions with high rock uplift rates. Combining parameters does not significantly improve the predictive power of the parameters for these drainages. In contrast to the Salween and Mekong River drainages, our proxy for climate (mean annual rainfall) best explains the variance in erosion rates in the Yangtze River drainage ($r^2 = 0.50$, $p < 0.01$; Fig. 6j–k), as we might expect for regions with lower rock uplift rates. Also in contrast to the Mekong and Salween watersheds (Fig. 6e, i), erosion rates in the Yangtze River drainage are correlated with basin area (Fig. 6k; $r^2 = 0.40$, $p < 0.01$). However, we suspect that this correlation is a result of sampling fewer small basins in the lower Yangtze rather than an inherent difference between the watersheds.

The analysis of mean local relief as a proxy for steepness and mean annual rainfall as a proxy for climate in the TRR shows that across a spatial decrease in inferred rock uplift rates, there is a transition from landscape steepness to climate being the best predictor of variance in erosion. That is, we observe a transition from mean local relief best explaining the variance in erosion rates in the Salween and Mekong River drainages to mean annual rainfall best explaining the variance in erosion rates in the Yangtze River drainage.

Our data from the TRR support the hypothesis that, other factors being equal, the relative influence of climate and topography on erosion rates changes as a function of rock uplift rate (see Section 1). Our Salween River data suggest that when rock uplift rates are high, variance in erosion rates is best explained by mean local relief. In contrast, in regions with low rates of rock uplift, variance in erosion rates will be best explained by rainfall, as we see in the Yangtze River basin.

While the shifting roles of landscape steepness and rainfall in driving erosion may help reconcile a number of results from previous studies, some areas do not follow this conceptual model. For example, in arid, tectonically active regions with extreme gradients in rainfall, researchers have found a correlation between rainfall and erosion rate (i.e., Jayko, 2005; Kober et al., 2007), likely due to the large gradient in rainfall overwhelming modest gradients in rock uplift. Other studies in tectonically active areas suggest that once hillslopes reach threshold steepness there will be a decoupling of erosion rates and mean local relief (see discussion in Section 1). In tectonically inactive areas such as passive margins and escarpments, other researchers have found no correlation between erosion rate and rainfall (i.e., Bierman and Caffee, 2001; Matmon et al., 2003a,b; Riebe et al., 2001; Vanacker et al., 2007; von Blanckenburg et al., 2004). However, these studies come from regions where erosion rates are controlled by a propagating base level fall, such as is typical along old escarpments. Hence, we propose that the

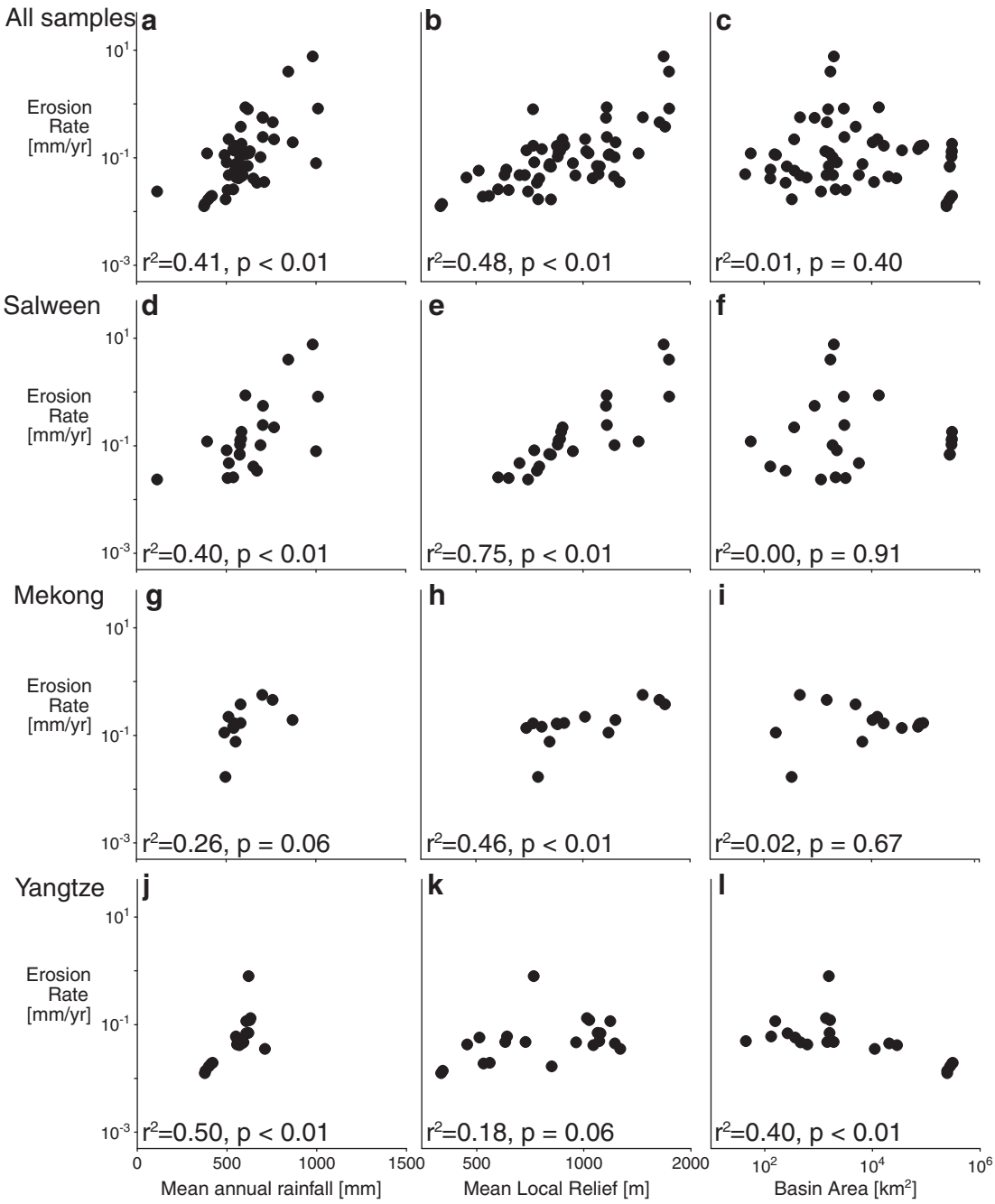

Fig. 6. Relationship between erosion rate and steepness and climatic parameters for each basin taken separately. Data for all basins is shown across the top row (a–c), Salween River is shown across second row (d–f), Mekong River in the third (g–i), and Yangtze River on the bottom (j–l). The left column shows erosion rate as a function of rainfall (a, d, g, j), the middle column shows erosion rate as a function of relief (b, e, h, k), and the far right column shows erosion rate as a function of basin area (c, f, i, l). Each plot shows the r^2 and p value for the single regression. For data on multiple regressions see data repository Table 5.

tectonic setting is the most important factor in determining whether climatic factors such as rainfall or the steepness of the landscape itself are better indicators of patterns of erosion rates.

4.3. Geomorphic mechanisms potentially controlling TRR erosion rates

The parallel eastward decrease in exhumation rates (and likely rock uplift) and millennial erosion rates across the lower TRR naturally leads to the question of how the Salween River is better able to incise its bed and evacuate the sediment shed from the hillslopes than the rivers to the east. What is the geomorphic mechanism by which the rivers can maintain the gradient in erosion rates we observe in the lower reaches of the TRR? Two geomorphic mechanisms have been proposed through which gradients in rock uplift may affect erosion rates by changing the efficiency of the river to incise.

One possibility is that proximity to the deformation front of the India–Asia collision resulted in increased erodibility of rocks in the Salween and Mekong Rivers relative to the Yangtze River. Molnar et al. (2007) suggest that tectonic activity could affect erosion rates through increased bedrock fracturing, thereby decreasing the resistance of the bedrock to erosion. As the relationship between erosion rate and fracturing is potentially highly non-linear, a large increase in erosion rate may result from a modest change in the fracture size or density of the bedrock. Although increased rock fracturing suggests a mechanism by which crustal deformation can affect erosion rates, it

does not address the question of whether steepness or climatic parameters correlates more strongly with measured erosion rates.

A second possibility is that in response to proximity to the India–Asia collision, the quantity of sediment stored on and protecting the bedrock bed of the rivers changes systematically from the Salween to the Yangtze River. Fluvial incision depends on the amount of sediment available to work as tools (and increase erosion) or armor the bed (and decrease erosion), and a river may respond to changing tectonic conditions through adjustments in the quantity of sediment on the river bed (Sklar and Dietrich, 2001). In the case of the TRR, assuming that the tools are limiting, the Salween River's higher erosion rate suggests that the sediment flux in the Salween River exceeds the flux in the Yangtze River, potentially enabling the Salween to sustain higher erosion rates.

Both the degree of rock fracturing and the availability of tools to erode bedrock riverbeds may contribute to the gradient in erosion rates across the lower TRR. With the data and tools at our disposal, we are unable to assess the relative contribution of each of these potential influences to erosion rates in the lower TRR.

5. Conclusions

Two strong spatial gradients are evident in the ^{10}Be-derived erosion rates in the TRR. First, as the rivers leave the low-relief surface of the Tibetan Plateau and become deeply incised into the steep, wet gorges in the lower basins, erosion rates predictably increase. Second, a steep transverse gradient in erosion rates exists across the TRR in the lower basins of each of the rivers where erosion rates are high. Here erosion rates decrease eastward by two orders of magnitude from the Salween to the Yangtze Rivers. Previous work on exhumation rates in areas to the east and west of the TRR suggests that there is a gradient in exhumation rate, and likely rock uplift, across this region. Our measured ^{10}Be erosion rates parallel this east–west decrease in long-term exhumation, and inferred rock uplift, rates across the lower basins of the TRR. On the timescales represented by the ^{10}Be erosion rates, we propose that differences in the tools available for incision or density of rock fracturing may enable rivers to respond to gradients in tectonic activity. We find that the relative importance of climate and steepness in setting millennial erosion rates changes across this gradient, suggesting the dominant control on erosion depends on rates of rock uplift.

Acknowledgements

We thank Greg Balco for help with analysis, many useful discussions during this project, and a helpful review of the paper, Joy Laydbak for help in lab, Patsy Garcia and John Weller for field work assistance, Harvey Greenberg for GIS help, and Josh Schmidt for help with figure revisions. The paper was improved significantly from constructive reviews by Marin Clark and an anonymous reviewer. This material is based upon work supported by the National Science Foundation under Grant No. EAR003561, the University of Washington Quaternary Research Center and Department of Earth and Space Sciences, the Geological Society of America Fahnestock Award, the Geological Society of America Mackin Award, and the UW Graduate School Top Scholar Award. Henck was supported by NSF-IGERT Grant No. 0333408 and an NSF Graduate Research Fellowship.

Appendix A. Supplementary data

Supplementary data to this article can be found online at doi:10.1016/j.epsl.2010.12.038.

References

Aalto, R., Dunne, T., Guyot, J.L., 2006. Geomorphic controls on Andean denudation rates. J. Geol. 114 (1), 85–99.

Ahnert, F., 1970. Functional relationships between denudation, relief, and uplift in large mid-latitude drainage basins. Am. J. Sci. 268, 243–263.

Akciz, S., Burchfiel, B.C., Crowley, J.L., Yin, J.Y., Chen, L.Z., 2008. Geometry, kinematics, and regional significance of the Chong Shan shear zone, Eastern Himlayan Syntaxis, Yunnan, China. Geosphere 4 (1), 292–314. doi:10.1130/GES00111.1.

Anders, A., Roe, G.H., Hallet, B., Montgomery, D.R., Finnegan, N., Putkonen, J., 2006. Spatial patterns of precipitation and topography in the Himalaya. In: Willett, S.D., Hovius, N., Brandon, M.T., Fisher, D. (Eds.), Tectonics, Climate, and Landscape Evolution. Geological Society of America, pp. 39–53. doi:10.1130/2006.2398(03).

Anders, A., Roe, G.H., Montgomery, D.R., Hallet, B., 2008. Influence of precipitation phase on the form of mountain ranges. Geology 36 (6), 479–482. doi:10.1130/G24821A.1.

Arne, D., Worley, B., Wilson, C., Chen, S.F., Foster, D., Luo, Z.L., Liu, S.G., Dirks, P., 1997. Differential exhumation in response to episodic thrusting along the eastern margin of the Tibetan Plateau. Tectonophysics 280, 239–256.

Balco, G., 2006. Converting Al and Be isotope ratio measurements to nuclide concentrations in quartz. *Documentation — Be-10/26-Al exposure age calculator*. http://hess.ess.washington.edu/math/docs/common/ams_data_reduction/2006Online.

Balco, G., Stone, J.O., Lifton, N.A., Dunai, T.J., 2008. A complete and easily accessible means of calculating surface exposure ages or erosion rates from Be-10 and Al-26 measurements. Quat. Geochronol. 3 (3), 174–195.

Barnes, J.B., Pelletier, J.D., 2006. Latitudinal variation of denudation in the evolution of the Bolivian Andes. Am. J. Sci. 306 (1), 1–31.

Bierman, P.R., 2004. Rock to sediment — slope to sea with Be-10 — rates of landscape change. Annu. Rev. Earth Planet. Sci. 32, 215–255.

Bierman, P.R., Caffee, M., 2001. Slow rates of rock surface erosion and sediment production across the Namib Desert and escarpment, southern Africa. Am. J. Sci. 301 (4–5), 326–358.

Bierman, P.R., Caffee, M., 2002. Cosmogenic exposure and erosion history of Australian bedrock landforms. Geol. Soc. Am. Bull. 114 (7), 787–803.

Bierman, P.R., Steig, E.J., 1996. Estimating rates of denudation using cosmogenic isotope abundances in sediment. Earth Surf. Process. Land. 21 (2), 125–139.

Binnie, S.A., Phillips, W.M., Summerfield, M.A., Fifield, L.K., 2007. Tectonic uplift, threshold hillslopes, and denudation rates in a developing mountain range. Geology 35 (8), 743–746. doi:10.1130/g23641a.

Booth, A.L., Zeitler, P.K., Kidd, W.S.F., Wooden, J., Liu, Y.P., Idleman, B., Hren, M., Chamberlain, C.P., 2004. U–Pb zircon constraints on the tectonic evolution of southeastern Tibet, Namche Barwa area. Am. J. Sci. 889–929.

Brown, E.T., Stallard, R.F., Larsen, M.C., Raisbeck, G.M., Yiou, F., 1995. Denudation rates determined from the accumulation of in situ-produced Be-10 in the Luquillo Experimental Forest, Puerto-Rico. Earth Planet. Sci. Lett. 129 (1–4), 193–202.

Burbank, D.W., Blythe, A.E., Putkonen, J., Pratt-Sitaula, B., Gabet, E., Oskin, M., Barros, A., Ojha, T.P., 2003. Decoupling of erosion and precipitation in the Himalayas. Nature 426 (6967), 652–655.

Burg, J.P., Davy, P., Nievergelt, P., Oberli, F., Seward, D., Diao, Z.Z., Meier, M., 1997. Exhumation during crustal folding in the Namche-Barwa syntaxis. Terra Nova 9 (2), 53–56.

Champagnac, J.D., Schlunegger, F., Norton, K., von Blanckenburg, F., Abbuhl, L.M., Schwab, M., 2009. Erosion-driven uplift of the modern Central Alps. Tectonophysics 474 (1–2), 236–249. doi:10.1016/j.tecto.2009.02.024.

Clark, M., Royden, L., 2000. Topographic ooze: building the eastern margin of Tibet by lower crustal flow. Geology 28 (8), 703–706.

Clark, M.K., Schoenbohm, L.M., Royden, L.H., Whipple, K.X., Burchfiel, B.C., Zhang, X., Tang, W., Wang, E., Chen, L., 2004. Surface uplift, tectonics, and erosion of eastern Tibet from large-scale drainage patterns. Tectonics 23 (1). doi:10.1029/2002TC001402.

Clark, M.K., Bush, J.W.M., Royden, L.H., 2005a. Dynamic topography produced by lower crustal flow against rheological strength heterogeneities bordering the Tibetan Plateau. Geophys. J. Int. 162, 575–590.

Clark, M.K., House, M.A., Royden, L.H., Whipple, K.X., Burchfiel, B.C., Zhang, X., Tang, W., 2005b. Late Cenozoic uplift of southeastern Tibet. Geology 33 (6), 525–528.

Clark, M., Royden, L., Whipple, K., Burchfiel, B., Zhang, X., Tang, W., 2006. Use of a regional, relict landscape to measure vertical deformation of the eastern Tibetan Plateau. J. Geophys. Res. Earth Surf. 111(F03002. doi:10.1029/2005JF000294.

Cyr, A.J., Granger, D.E., 2008. Dynamic equilibrium among erosion, river incision, and coastal uplift in the northern and central Apennines, Italy. Geology 36 (2), 103–106. doi:10.1130/g24003a.1.

Demoulin, A., Hallot, E., Rixhon, G., 2009. Amount and controls of the Quaternary denudation in the Ardennes massif (western Europe). Earth Surf. Process. Land. 34 (11), 1487–1496. doi:10.1002/esp. 1834.

Ding, L., Zhong, D.L., Yin, A., Kapp, P., Harrison, T.M., 2001. Cenozoic structural and metamorphic evolution of the eastern Himalayan syntaxis (Namche Barwa). Earth Planet. Sci. Lett. 192 (423–438).

Dixon, J.L., Heimsath, A.M., Amundson, R., 2009. The critical role of climate and saprolite weathering in landscape evolution. Earth Surf. Process. Land. 34 (11), 1507–1521.

Duvall, A., Kirby, E., Burbank, D., 2004. Tectonic and lithologic controls on bedrock channel profiles and processes in coastal California. J. Geophys. Res. Earth Surf. 109 (F3, F03002. doi:10.1029/2003jf000086.

Enkelmann, E., Ratschbacher, L., Johnckheere, R., Nestler, R., Fleischer, M., Gloaguen, R., Hacker, B., Zhang, Y.Q., Ma, Y.S., 2006. Cenozoic exhumation and deformation of northeastern Tibet and the Qinling; is Tibetan lower crustal flow diverging around the Sichuan Basin? Geol. Soc. Am. Bull. 118 (5–6), 651–671.

Finlayson, D.P., Montgomery, D.R., Hallet, B., 2002. Spatial coincidence of rapid inferred erosion with young metamorphic massifs in the Himalayas. Geology 30 (3), 219–222.

Finnegan, N.J., Roe, G., Montgomery, D.R., Hallet, B., 2005. Controls on the channel width of rivers: implications for modeling fluvial incision of bedrock. Geology 33 (3), 229–232.
Finnegan, N.J., Hallet, B., Montgomery, D.R., Zeitler, P.K., Stone, J., Anders, A., Liu, Y., 2008. Coupling of rock uplift and river incision in the Namche Barwa-Gyala Peri massif, Tibet. Geol. Soc. Am. Bull. 120 (1–2), 142–155. doi:10.1130/B226224.1.
Gilley, L.D., Harrison, T.M., Leloup, P.H., Ryerson, F.J., Lovera, O.M., Wang, J.H., 2003. Direct dating of left-lateral deformation along the Red River shear zone, China and Vietnam. J. Geophys. Res. Solid Earth 108(B2. doi:10.1029/2001JB001726.
Godard, V., Pik, R., Lave, J., Cattin, R., Tibari, B., de Sigoyer, J., Pubellier, M., Zhu, J., 2009. Late Cenozoic evolution of the central Longmen Shan, eastern Tibet: insight from (U–Th)/He thermochronometry. Tectonics 28, Tc5009. doi:10.1029/2008tc002407.
Granger, D.E., Kirchner, J.W., Finkel, R., 1996. Spatially averaged long-term erosion rates measured from in situ-produced cosmogenic nuclides in alluvial sediment. J. Geol. 104 (3), 249–257.
Hallet, B., Molnar, P., 2001. Distorted drainage basins as markers of crustal strain east of the Himalaya. J. Geophys. Res. Solid Earth 106(B7, 13697–13709.
Harkins, N., Kirby, E., Heimsath, A., Robinson, R., Reiser, U., 2007. Transient fluvial incision in the headwaters of the Yellow River, northeastern Tibet, China. J. Geophys. Res. Earth Surf. 112(F3), F03S04. doi:10.1029/2006JF000570.
Harrison, T.M., Chen, W.J., Leloup, P.H., Ryerson, F.J., Tapponnier, P., 1992. An Early Miocene transition in deformation regime within the Red River Fault Zone, Yunnan and its significance for Indo-Asian tectonics. J. Geophys. Res. Solid Earth 97(B5, 7159–7182.
Jayko, A.S., 2005. Late Quaternary denudation, Death and Panamint Valleys, eastern California. Earth Sci. Rev. 73 (1–4), 271–289.
Kirby, E., Reiners, P.W., Krol, M.A., Whipple, K.X., Hodges, K.V., Farley, K.A., Tang, W.Q., Chen, Z.L., 2002. Late Cenozoic evolution of the eastern margin of the Tibetan Plateau: inferences from Ar-40/Ar-39 and (U–Th)/He thermochronology. Tectonics 21 (1). doi:10.1029/2000TC001246.
Kober, F., Ivy-Ochs, S., Schlunegger, F., Baur, H., Kubik, P.W., Wieler, R., 2007. Denudation rates and a topography-driven rainfall threshold in northern Chile: multiple cosmogenic nuclide data and sediment yield budgets. Geomorphology 83 (1–2), 97–120.
Kohl, C.P., Nishiizumi, K., 1992. Chemical isolation of quartz for measurement of insitu-produced cosmogenic nuclides. Geochim. Cosmochim. Acta 56 (9), 3583–3587.
Kong, P., Na, C.G., Fink, D., Ding, L., Huang, F.X., 2007. Erosion in northwest Tibet from in-situ-produced cosmogenic Be-10 and Al-26 in bedrock. Earth Surf. Process. Land. 32 (1), 116–125.
Lacassin, R., Scharer, U., Leloup, P.H., Arnaud, N., Tapponnier, P., Liu, X.H., Zhang, L.S., 1996. Tertiary deformation and metamorphism SE of Tibet: the folded tiger-leap decollement of NW Yunnan, China. Tectonics 15 (3), 605–622. doi:10.1029/95TC03749.
Lal, D., Harris, N.B.W., Sharma, K.K., Gu, Z.Y., Ding, L., Liu, T.S., Dongal, W.Q., Caffee, M.W., Jull, A.J.T., 2004. Erosion history of the Tibetan Plateau since the last interglacial: constraints from the first studies of cosmogenic Be-10 from Tibetan bedrock. Earth Planet. Sci. Lett. 217 (1–2), 33–42. doi:10.1016/s0012-821x(03)00600-9.
Leloup, P.H., Kienast, J.R., 1993. High-temperature metamorphism in a major strike-slip shear zone: the Ailao Shan-Red River, People's Republic of China. Earth Planet. Sci. Lett. 118, 213–234.
Leloup, P.H., Lacassin, R., Tapponnier, P., Scharer, U., Zhong, D.L., Liu, X.H., Zhang, L.S., Ji, S.C., Trinh, P.T., 1995. The Ailao Shan-Red River shear zone (Yunnan, China), Tertiary transform boundary of Indochina. Tectonophysics 251 (1–4), 3–10.
Leloup, P.H., Arnaud, N., Lacassin, R., Kienast, J.R., Harrison, T.M., Phan Trong, T.T., Replumaz, A., Tapponnier, P., 2001. New constraints on the structure, thermochronology, and timing of the Ailao Shan-Red River shear zone, SE Asia. J. Geophys. Res. Solid Earth 106, 6683–6732.
Liu-Zeng, J., Tapponnier, P., Gaudemer, Y., Ding, L., 2008. Quantifying landscape differences across the Tibetan plateau: implications for topographic relief evolution. J. Geophys. Res. Earth Surf. 113(F4), F04018. doi:10.1029/2007jf000897.
Malloy, M.A., 2004. Rapid Erosion at the Tsangpo Knickpoint and Exhumation of Southeastern Tibet. MS, Earth and Environmental Sciences, Lehigh University.
Matmon, A., Bierman, P.R., Larsen, J., Southworth, S., Pavich, M., Caffee, M., 2003a. Temporally and spatially uniform rates of erosion in the southern Appalachian Great Smoky Mountains. Geology 31 (2), 155–158.
Matmon, A., Bierman, P.R., Larsen, J., Southworth, S., Pavich, M., Finkel, R., Caffee, M., 2003b. Erosion of an ancient mountain range, the Great Smoky Mountains, North Carolina and Tennessee. Am. J. Sci. 303 (9), 817–855.
Molnar, P., Anderson, R.S., Anderson, S.P., 2007. Tectonics, fracturing of rock, and erosion. J. Geophys. Res. Earth Surf. 112(F3). doi:10.1029/2005JF000433.
Montgomery, D.R., Brandon, M.T., 2002. Topographic controls on erosion rates in tectonically active mountain ranges. Earth Planet. Sci. Lett. 201 (3–4), 481–489.
Montgomery, D.R., Balco, G., Willett, S.D., 2001. Climate, tectonics, and the morphology of the Andes. Geology 29 (7), 579–582.
Mora, A., Parra, M., Strecker, M.R., Sobel, E.R., Hooghiemstra, H., Torres, V., Jaramillo, J.V., 2008. Climatic forcing of asymmetric orogenic evolution in the Eastern Cordillera of Colombia. Geol. Soc. Am. Bull. 120 (7–8), 930–949.
Nishiizumi, K., Imamura, M., Caffee, M.W., Southon, J.R., Finkel, R.C., McAninch, J., 2007. Absolute calibration of Be-10 AMS standards. Nucl. Instrum. Methods Phys. Res. Sect. B 258 (2), 403–413.
Ouimet, W.B., Whipple, K.X., Granger, D.E., 2009. Beyond threshold hillslopes: channel adjustment to base-level fall in tectonically active mountain ranges. Geology 37 (7), 579–582. doi:10.1130/G30013A.1.
Ouimet, W.B., Whipple, K.X., Royden, L.H., Reiners, P., Hodges, K., Pringle, M.S., 2010. Regional incision of the eastern margin of the Tibetan Plateau. Lithosphere 2 (1), 50–63. doi:10.1130/L57.1.
Quigley, M., Sandiford, M., Fifield, L.K., Alimanovic, A., 2007. Landscape responses to intraplate tectonism: quantitative constraints from Be-10 nuclide abundances. Earth Planet. Sci. Lett. 261 (1–2), 120–133. doi:10.1016/j.epsl.2007.06.020.
Reid, A.J., Wilson, C.J.L., Phillips, D., Liu, S., 2005. Mesozoic cooling across the Yidun Arc, central-eastern Tibetan Plateau: a reconnaissance 40Ar/39Ar study. Tectonophysics 398, 45–66.
Reiners, P.W., Ehlers, T.A., Mitchell, S.G., Montgomery, D.R., 2003. Coupled spatial variations in precipitation and long-term erosion rates across the Washington Cascades. Nature 426 (6967), 645–647.
Riebe, C.S., Kirchner, J.W., Granger, D.E., Finkel, R.C., 2001. Minimal climatic control on erosion rates in the Sierra Nevada, California. Geology 29 (5), 447–450.
Roering, J.J., Kirchner, J.W., Dietrich, W.E., 1999. Evidence for nonlinear, diffusive sediment transport on hillslopes and implications for landscape morphology. Water Resour. Res. 35 (3), 853–870.
Royden, L.H., Burchfiel, B.C., King, R.W., Wang, E., Chen, Z.L., Shen, F., Liu, Y.P., 1997. Surface deformation and lower crustal flow in eastern Tibet. Science 276 (5313), 788–790.
Safran, E.B., Bierman, P.R., Aalto, R., Dunne, T., Whipple, K.X., Caffee, M., 2005. Erosion rates driven by channel network incision in the Bolivian Andes. Earth Surf. Process. Land. 30 (8), 1007–1024.
Scharer, U., Tapponnier, P., Lacassin, R., Leloup, P.H., Zhong, D.L., Ji, S.C., 1990. Intraplate tectonics in Asia: a precise age for large-scale Miocene movement along the Ailao Shan-Red River shear zone, China. Earth Planet. Sci. Lett. 97, 65–77.
Schoenbohm, L.M., Whipple, K.X., Burchfiel, B.C., Chen, L., 2004. Geomorphic constraints on surface uplift, exhumation, and plateau growth in the Red River region, Yunnan Province, China. Geol. Soc. Am. Bull. 116 (7–8), 895–909.
Schoenbohm, L.M., Burchfiel, B.C., Chen, L.Z., 2006a. Propagation of surface uplift, lower crustal flow, and Cenozoic tectonics of the southeast margin of the Tibetan Plateau. Geology 34 (10), 813–816. doi:10.1130/G22625.1.
Schoenbohm, L.M., Burchfiel, B.C., Chen, L.Z., Yin, J.Y., 2006b. Miocene to present activity along the Red River fault, China, in the context of continental extrusion, upper-crustal rotation, and lower-crustal flow. Geol. Soc. Am. Bull. 118 (5–6), 672–688. doi:10.1130/B25816.1.
Seward, D., Burg, J.P., 2008. Growth of the Namche Barwa Syntaxis and associate evolution of the Tsangpo Gorge: constraints from structural and thermochronological data. Tectonophysics 451, 282–289 10.1016.
Sklar, L.S., Dietrich, W.E., 2001. Sediment and rock strength controls on river incision into bedrock. Geology 29 (12), 1087–1090.
Sol, S., Meltzer, A.S., Burgmann, R., Van der Hilst, R., King, R.W., Chen, Z., Koons, P.O., Lev, E., Liu, Y.P., Zeitler, P.K., Zhang, X., Zhang, J., Zurek, B., 2007. Geodynamics of the southeastern Tibetan Plateau from seismic anisotropy and geodesy. Geology 35 (6), 563–566.
Stewart, R.J., Hallet, B., Zeitler, P.K., Malloy, M.A., Allen, C.M., Trippett, D., 2008. Brahmaputra sediment flux dominated by highly localized rapid erosion from the easternmost Himalaya. Geology 36 (9), 711–714. doi:10.1130/G24890A.1.
Stock, J.D., Montgomery, D.R., 1999. Geologic constraints on bedrock river incision using the stream power law. J. Geophys. Res. 104, 4983–4993.
Stone, J.O., 2004. Extraction of Al and Be from quartz for isotopic analysis. UW Cosmogenic Nuclide Lab Meth. Proced.http://depts.washington.edu/cosmolab/chem.html Online.
Tapponnier, P., Xu, Z.Q., Roger, F., Meyer, B., Arnaud, N., Wittlinger, G., Yang, J.S., 2001. Geology — oblique stepwise rise and growth of the Tibet plateau. Science 294 (5547), 1671–1677.
Taylor, M., Yin, A., 2009. Active structures of the Himalayan–Tibetan orogen and their relationships to earthquake distribution, contemporary strain field, and Cenozoic volcanism. Geosphere 5 (3), 199–214. doi:10.1130/GES00217.1.
Tomkins, K.M., Humphreys, G.S., Wilkinson, M.T., Fink, D., Hesse, P.P., Doerr, S.H., Shakesby, R.A., Wallbrink, P.J., Blake, W.H., 2007. Contemporary versus long-term denudation along a passive plate margin: the role of extreme events. Earth Surf. Process. Land. 32 (7), 1013–1031.
USGS, 2001. Global GIS database: digital atlas of South Asia. In: Hearn, J.P., Hare, T., Schruben, P., Sherrill, D., LaMar, C., Tsushima, P. (Eds.), Global GIS Database, Digital Data Series DDS-62-C: USGS.
USGS, 2008. HydroSHEDS. World Wildlife Fund. (WWF) online http://hydrosheds.cr.usgs.gov/. date accessed: 22 Jan 2009.
Vanacker, V., von Blanckenburg, F., Hewawasam, T., Kubik, P.W., 2007. Constraining landscape development of the Sri Lankan escarpment with cosmogenic nuclides in river sediment. Earth Planet. Sci. Lett. 253 (3–4), 402–414.
Vance, D., Bickle, M., Ivy-Ochs, S., Kubik, P.W., 2003. Erosion and exhumation in the Himalaya from cosmogenic isotope inventories of river sediments. Earth Planet. Sci. Lett. 206 (3–4), 273–288.
von Blanckenburg, F., 2005. The control mechanisms of erosion and weathering at basin scale from cosmogenic nuclides in river sediment. Earth Planet. Sci. Lett. 237 (3–4), 462–479.
von Blanckenburg, F., Hewawasam, T., Kubik, P.W., 2004. Cosmogenic nuclide evidence for low weathering and denudation in the wet, tropical highlands of Sri Lanka. J. Geophys. Res. Earth Surf. 109(F3, F03008. doi:10.1029/2003jf000049.
Whipple, K.X., Tucker, G.E., 1999. Dynamics of the stream-power river incision model: implications for height limits of mountain ranges, landscape response timescales, and research needs. J. Geophys. Res. Solid Earth 104(B8, 17661–17674.
Wittmann, H., von Blanckenburg, F., Kruesmann, T., Norton, K.P., Kubik, P.W., 2007. Relation between rock uplift and denudation from cosmogenic nuclides in river

sediment in the Central Alps of Switzerland. J. Geophys. Res. Earth Surf. 112(F4, F04010. doi:10.1029/2006jf000729.
Xu, G.Q., Kamp, P.J.J., 2000. Tectonics and denudation adjacent to the Xianshuihe Fault, eastern Tibetan Plateau: constraints from fission track thermochronology. J. Geophys. Res. Solid Earth 105(B8, 19231–19251.
Yin, A., Harrison, T.M., 2000. Geologic evolution of the Himalayan–Tibetan Orogen. Annu. Rev. Earth Planet. Sci. 28, 211–280.
Zeitler, P.K., Meltzer, A.S., Koons, P.O., Craw, D., Hallet, B., Chamberlain, C.P., Kidd, W.S.F., Park, S.K., Seeber, L., Bishop, M., Shroder, J., 2001. Erosion, Himalayan geodynamics, and the geomorphology of metamorphism. GSA Today 11 (1), 4–9.
Zhang, P.Z., Shen, Z., Wang, M., Gan, W.J., Burgmann, R., Molnar, P., 2004. Continuous deformation of the Tibetan Plateau from global positioning system data. Geology 32 (9), 809–812.